Available online at www.sciencedirect.com
ScienceDirect
Journal of Nuclear Materials 363–365 (2007) 703–707
journal of nuclear materials
www.elsevier.com/locate/jnucmat

Reynolds stress and edge turbulence in TEXTOR: A comparison between simulations and experiment

M. Vergote *, M. Van Schoor, Y. Xu, S. Jachmich, R. Weynants

Association 'Euratom-Etat Belge' – Associatie 'Euratom-Belgische Staat', Ecole Royale Militaire – Koninklijke Militaire School, Avenue de la Renaissance, Renaissancelaan 30, B-1000 Brussels, Belgium

Abstract

We discuss the modeling of turbulence by means of a simulation code and compare these simulations to experimental results recently obtained in TEXTOR using a new Reynolds stress probe. The probe, reciprocating on a fast manipulator, allows to track poloidal and radial electric field and density fluctuations, which permits us to compute the (E × B)-velocity fluctuations as well as the Reynolds stress, the fluctuation driven particle fluxes and correlation functions. The simulations are based on the Hasegawa–Wakatani model, completed with curvature and neutral drag terms. We further investigate the potential role Reynolds stresses play in driving or damping the background flows, with the aid of a one dimensional fluid model in which the toroidal geometry is correctly taken into account, while various sources and sinks like viscosity, interaction with neutrals and Reynolds stresses are included.

PACS: 52.35.Ra; 52.25.Fi; 52.55.Fa

Keywords: Textor; Turbulence; Cross field transport; Edge modeling

1. Introduction

It is generally accepted that turbulence is responsible for the experimentally observed anomalous transport in tokamaks. Also well known is the fact that turbulence can be quenched by sheared flows which rip the convective cells apart, thus forming a barrier. The opposite mechanism of the turbulence generating a macroscopical sheared or a zonal flow (large scale structure with $k_\theta \ll k_r$) has been studied as well, both on the theoretical [1] and experimental side [2,3]. In this paper we will confront experimental data from probe measurements in the edge of TEXTOR with 2 models. The first one is a turbulence model based on the Hasegawa–Wakatani (H–W) equations and is used to simulate the locally measured turbulence. We want to keep the turbulence model as simple as possible and we choose a slab representation as in Ref. [4] with $q = \infty$ and without magnetic shear. The outcome of these simulations is compared to experimental values of the turbulence measurements on TEXTOR. For this we dispose of a new Reynolds stress probe mounted on a fast reciprocating manipulator located at the

* Corresponding author. Fax: +32 2 735 24 21.
E-mail address: Maarten.Vergote@rma.ac.be (M. Vergote).

0022-3115/$ - see front matter © 2007 Elsevier B.V. All rights reserved.
doi:10.1016/j.jnucmat.2007.01.142

outboard equator ($\theta = 0$), as reported in [5] and similar to the probe described in [6].

With the probe we are able to measure the plasma's poloidal background rotation as well; so we can investigate up to which level this background flow could be driven by the observed Reynolds stress. To this end we built a second model [6] for the rotation in which we introduce different driving and damping mechanisms, taking into account the correct toroidal geometry.

2. Turbulence modeling

We choose the H–W equations as a paradigm to simulate locally the turbulence that is experimentally measured at the edge of TEXTOR. To the original H–W model [7], we added curvature terms representing the local, moderate effect of the curved and inhomogeneous magnetic field [8], as well as particle diffusion in the electron continuity equation and a neutral drag term in the vorticity equation. With the proper non-dimensional definition of the fluctuating density $n' = \frac{n}{n_0}$ and the potential $\phi' = \frac{e\phi}{k_B T}$, we can write our model equations:

$$\frac{\mathrm{d}_E}{\mathrm{d}t'}\nabla_\perp'^2\phi' = -v^*\nabla_\perp'^2\phi' + C_1(\phi' - n') - \mathscr{K}'(n') + C_2\nabla_\perp'^2(\nabla_\perp'^2\phi'), \tag{1}$$

$$\frac{\mathrm{d}_E}{\mathrm{d}t'}n' = -\kappa_n\frac{\partial\phi'}{\partial y'} + C_1(\phi' - n') + \mathscr{K}'(\phi' - n') + C_2\nabla_\perp'^2 n' \tag{2}$$

in which the primes denote dimensionless quantities ($x' = x/\rho_s$, $y' = y/\rho_s$, $t' = \omega_{ci}t$, with ω_{ci} the ion gyro-frequency and ρ_s the ion Larmor radius at electron temperature) and $\frac{\mathrm{d}_E}{\mathrm{d}t'} = \frac{\partial}{\partial t'} + [\phi',]$ is the total time derivative, in which the advecting $\vec{\mathbf{E}} \times \vec{\mathbf{B}}$-velocity appears in the Poisson brackets $[\phi', \bullet] = [\frac{\partial\phi'}{\partial x'}\frac{\partial}{\partial y'} - \frac{\partial\phi'}{\partial y'}\frac{\partial}{\partial x'}]\bullet$. The normalized background density gradient is written as $\kappa_n = |\frac{\partial(\ln n_o)}{\partial x'}| = \frac{\rho_s}{L_n}$ and the curvature in the equatorial plane at the low field side (LFS) as an operator $\mathscr{K}'(f) = \omega_B\frac{\partial f}{\partial y'}$, with $\omega_B = \frac{2\rho_s}{R_o}$ [9,8]. The parallel coupling is abbreviated by $C_1 = \frac{kT_e\sigma_z}{e^2\omega_{ci}n_o}k_z^2$ (with σ_z the electron conductivity in the parallel direction, and the parallel wavenumber k_z) and the kinematic ion shear viscosity μ is introduced by $C_2 = \frac{\mu}{\omega_{ci}\rho_s^2}$. In the neutral friction coefficient $v^* = n_n\langle\sigma.v\rangle$ [10] the neutral density n_n is supposed constant.

We do not expect the ballooning mechanism to be important, because the ballooning parameter $v_B = \frac{m_e}{M_i}\frac{q^2R_0v_e}{c_s} = 0.1 < 1$ for our TEXTOR parameters (see below; q is the safety factor, R_0 the major radius, v_e the electron collision frequency and $c_s = \sqrt{T_e/M_i}$ the sound speed) [11]. As a consequence, for a simple simulation-model a two dimensional (2D) approach can suffice. Moreover, local 3D dynamics were investigated by Biskamp in [4]: it appears that the k_z spectrum evolves towards a spectrum where the smallest k_z-components are dominant. As k_z cannot be exactly zero over a range of radii, we thus take an appropriately small but nonzero k_z to obtain $C_1 = C_{1,cst}$. Thus we suppose that the turbulence close to the separatrix and the scrape off layer is nearly 2D, and we solve the H–W equations in 2D. The choice of k_z (or equivalently C_1) is important: we investigated next to the reference runs with $k_z \approx (qR)^{-1}$ (or $C_1 = 0.3\kappa_n$), two scenarios with even smaller k_z: $C_1 = 0.1\kappa_n$ and $C_1 = 0.05\kappa_n$, with and without curvature. The coefficients C_2, v^* and ω_B used in the simulations are determined according to the edge parameters of TEXTOR (Deuterium as working gas, n_n is 1% of n_0, $T_e \approx 40$ eV, $n_0 = 5\times10^{18}\,\mathrm{m}^{-3}$, $\nabla n_o = -1\times10^{20}m^{-4}$ and $R_o = 1.75$ m, minor radius $a = 0.47$ m, $B_T = 1.9$T). The evolution of these dynamical equations is computed locally by a pseudospectral code on a xy-grid with periodic boundary conditions (x representing the minor radial direction r). The maximum dimensionless wavenumber is typically 4π, ensuring well-resolved turbulence. The time stepping algorithm is based on the Karniadakis IMEX-scheme [12]. To compare with the data taken at TEXTOR, we put 'probe pins' in the simulation grid of 32×64 ρ_s (sometimes 16×32 ρ_s) and sample the numerical signals from the simulation in the same way as is done in the experiment (500 kHz).

With these coefficients ($\kappa_n = 0.012$, $0.05\kappa_n \leqslant C_1 \leqslant 0.3\kappa_n$, $\omega_B = 7\times10^{-4}$, $v^* = 2\times10^{-5}$ and $C_2 = 2\times10^{-5}$) we still find the typical drift wave behavior in the early linear stage: starting from a standard low-amplitude k-spectrum (as in Ref. [7]), the drift waves first grow linearly at $k'_x \approx 0$, $k'_y \approx 1$ until they reach a saturation level evolving in a highly nonlinear turbulent regime (from $t' \approx 6000$ on, see Fig. 1). Once the saturation is started the energy condenses in the larger scales via the non-linear coupling and the moderate linear interchange drive. We can distinguish different transport behaviors for different values of the parallel coupling. The value of the diffusion coefficient for $C_1 = 0.3\kappa_n$ is three times lower than that for $C_1 = 0.05\kappa_n$. Furthermore we observe more intermittent behavior in the latter case, mostly in the run with curvature in the model; the red colored run (color online) for $C_1 = 0.05\kappa_n$

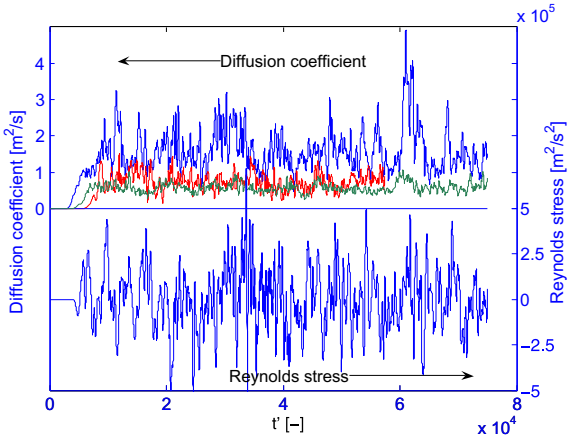

Fig. 1. Time trace of the simulations for 1% of neutrals. Up: spectrally calculated diffusion coefficient $D = \langle n\, v_x \rangle$ for $C_1 = 0.05\kappa_n$ (blue), $C_1 = 0.05\kappa_n$ without curvature (red) and $C_1 = 0.3\kappa_n$ (green). Down: Reynolds stress $\langle v_x v_y \rangle$ for $C_1 = 0.05\kappa_n$ (For interpretation of the references to color in this figure legend, the reader is referred to the web version of this article.).

without curvature (or $\omega_B = 0$) and which was stopped at $t' \approx 5.5 \times 10^4$, is more quiescent. Whereas the interchange terms have a negligible influence for $C_1 = 0.3\kappa_n$ and even for $C_1 = 0.1\kappa_n$, they do contribute relatively much for $C_1 = 0.05\kappa_n$.

The importance of neutral damping becomes only significant when the fraction $n_n > 0.10 n_0$, adding a non-negligible sink over the whole spectrum. We ran two more cases different from the reference scenario ($C_1 = 0.3\kappa_n$) with the realistic fraction $n_n = 1\%$: $n_n = 10\%$ and $n_n = 50\%$. It is only in the last case that the transport (diffusion coefficient and Reynolds stress) is reduced. We see a reduction of D with 25% once the neutral fraction attains 50%.

We can now also compare this result to the experiment. As our simulation model does not contain any imposed background poloidal flow, we compare with the data of a radial position in the machine where v_θ is small ($r \approx 43$ cm, see [13]). The absolute value of the anomalous particle diffusion in TEXTOR (at this radius) is $D \approx 0.3\ \mathrm{m^2/s}$ and this corresponds rather well with the result of the simulation for $C_1 = 0.3\kappa_n$ ($D \approx 0.5$, see Fig. 1 (up)). The two other scenarios with $C_1 = 0.1\kappa_n$ and $C_1 = 0.05\kappa_n$ give, respectively, 1 and 1.5. Concerning the potential and density fluctuations individually, we find almost perfect agreement for the smallest C_1 value (less than a factor of 2 of difference), whereas there is a factor of 4 of difference between the experiment and the too small fluctuations for $C_1 = 0.3\kappa_n$. We believe that the assumption of isothermal electrons and cold ions are the major reason for this underestimation of the fluctuation levels.

The fact that too low individual fluctuations can nevertheless result in a rather good correspondence of the particle transport, can be explained by the difference in phase between n and ϕ which is too small; experimentally we have a cross correlation of about $0.1 - 0.3$ (depending on the minor radius), whereas we find for $C_1 = 0.3\kappa_n$ a value of 0.8 and for $C_1 = 0.05\kappa_n$ a value of 0.6. Taking into account the fact that background poloidal flow shear generally lowers this cross correlation, we can conclude that the values of C_1 to apply this model, are quite appropriate.

Concerning the transport of momentum, we measure on TEXTOR experimentally Reynolds stresses of the order of $10^6\ \mathrm{m^2/s^2}$. Comparing this to the values of Fig. 1, $\langle v_r v_\theta \rangle_{rms} \approx 4 \times 10^5$ makes us conclude that this is consistent with the factor of 2 in the individual fluctuations (best agreement for $C_1 = 0.05\kappa_n$, a factor of 3–4 too low).

Furthermore we have to note that the real probe is characterized by an array of pins separated $\Delta_\theta = 3$mm poloidally and $\Delta_r = 4$ mm radially [5], so that the experimentally measurable wavenumbers are limited to $k_{\theta,\max} = \pi/\Delta_\theta \approx 1000\ \mathrm{m^{-1}}$. A typical wavenumber spectrum from TEXTOR (at $r \approx 43$ cm for ohmic data) is compared to the simulated spectrum in Fig. 2.

On the very large scales ($|k_\theta| < 50\ \mathrm{m^{-1}}$), one sees dominant components in TEXTOR. These can be associated to the lowest-frequency zonal flows (about 5 kHz) and their harmonics. These lower wavenumbers ($|k_\theta| < 1000\ \mathrm{m^{-1}}$) are not sufficiently present in our highly resolved simulations ($k_\theta \in [160, 2 \times 10^4]$, see Fig. 2(b): simul, instantaneous spectrum), unless we take an even larger domain, demanding more computing power and the correct implementation of the toroidal geometry. Therefore the comparison should be done with some care, but the tendency of the spectrum of the simulation (Fig. 2(a) and (b) for the whole domain) fits rather well the behavior of the experimental spectrum. The too low amplitude of $S_{\mathrm{simul}}(k_\theta)$ for $k_\theta < 700\ \mathrm{m^{-1}}$ reflects this shortcoming.

In conclusion, we can state that a simple 2D model like H–W with curvature can approximate the turbulence in the edge up to one order of magnitude. For $C_1 = 0.3\kappa_n$, we find fluctuation levels that are too low and a close relationship between n and ϕ resulting in a particle transport of the order

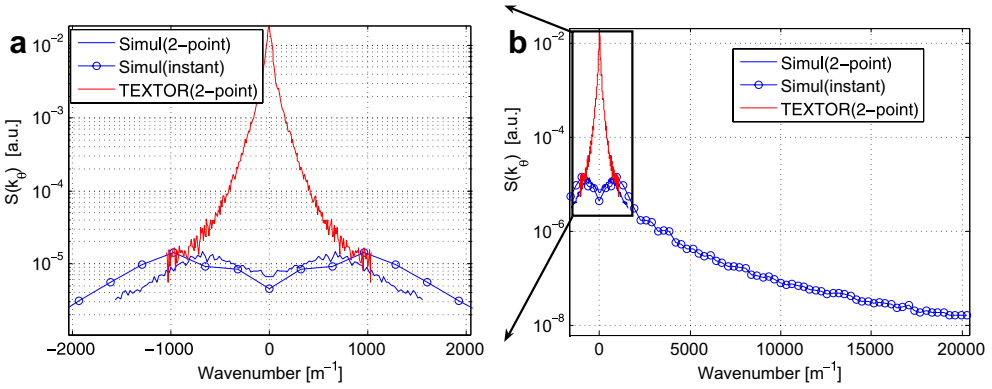

Fig. 2. (See color online). (a) Wavenumber spectrum in TEXTOR at $r \approx 43$ cm and from the simulation $C_1 = 0.3\kappa_n$ (- - : computed via the 2-point correlation technique [14], —o— : instantaneous). (b) Comparison of the covered domains.

of the real value. The runs with $C_1 = 0.05\kappa_n$ show a better agreement on the fluctuation levels and momentum transport, a more realistic cross correlation and slightly overestimated particle transport.

3. Poloidal flows driven by Reynolds stress

To study the macroscopical influence of the Reynolds stress on the $m = r \cdot k_\theta = 0$ poloidal rotation in the edge, we follow a Reynolds decomposition and write the fluid velocity $\vec{\mathbf{v}}$ and the density n as a mean plus a fluctuating part ($\vec{\mathbf{v}} = \underline{\vec{\mathbf{v}}} + \underset{\sim}{\vec{\mathbf{v}}}$, $n = \underline{n} + \underset{\sim}{n}$ with the time-average $\underline{x} = \langle x \rangle_\tau = \frac{1}{\tau}\int_0^\tau x(t)\mathrm{d}t$ over the timescale of averaging τ which is large compared to the timescale of the fluctuations, but short with respect to any macroscopical timescale). Projecting the total momentum equation, with $\vec{\mathbf{U}} = \underline{\vec{\mathbf{v}}} + \frac{\overset{n}{\underset{\sim}{\underset{\sim}{\vec{\mathbf{v}}}}}}{\underline{n}}$ as a total fluid velocity, on the toroidal and parallel direction and averaging over the flux surface in a simple tokamak geometry, leads to an equation for $F(r)/R_0$, the flux-surface-averaged poloidal velocity [6]. As we only wish to model a narrow radial layer we take $q \approx 4.5$ to be constant, and we find:

$$\frac{\partial}{\partial t}\left(\frac{F(r)}{R_0}\right) = -\frac{1}{\underline{n}(1+2q^2)}\frac{1}{r^2}\frac{\partial}{\partial r}\left(r^2\underline{n}\underset{\sim}{\underset{\sim}{(v_r v_\theta)}}\right) - \nu^*\frac{F(r)}{R_0} - \frac{1}{\underline{n}\Theta m B_0(1+2q^2)}C\left(\frac{F(r)}{R_0} - U_{Neo}\right). \quad (3)$$

In this equation, the convection has been neglected and the viscosity is reduced to $\langle \vec{\mathbf{B}} \cdot \vec{\nabla} \cdot \vec{\vec{\pi}} \rangle_{\mathrm{flux}} = C \cdot \left(\frac{F(r)}{R_o} - U_{Neo}\right)$ where we take a general expression

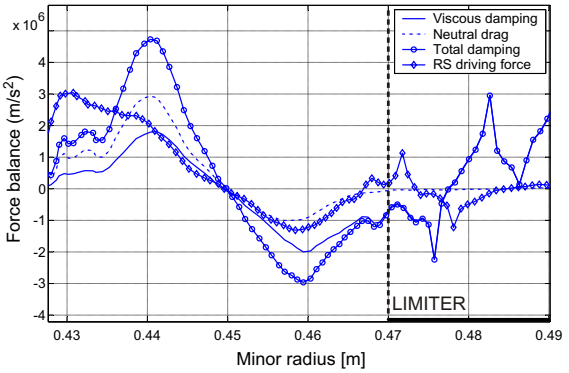

Fig. 3. Comparison between the different terms in Eq. (3).

for C given in [15] and $U_{Neo} = \frac{-2.1}{ZeB_o}(\partial T_i/\partial r)$ [16]. A neutral fraction of 2% is supposed at the separatrix with a decay length of 2.5 cm inwards [17], compatible with the 1% previously used at $r = 43$ cm. In case of stationarity ($\frac{\partial}{\partial t} = 0$) the off-diagonal element of the Reynolds stress tensor $\underset{\sim}{\underset{\sim}{(v_r v_\theta)}}$ is the only possible driving force that can sustain the poloidal velocity (if it exhibits a radial gradient) to balance the viscous friction and neutral drag.

To compare these three forces, we use the experimentally measured values of the Reynolds stress and the poloidal velocity, which is dominated by the $\vec{\mathbf{E}} \times \vec{\mathbf{B}}$ -velocity.

In Fig. 3, we see a rather good correspondence between the Reynolds stress driving term and the sum of the damping terms (third and fourth terms of Eq. (3) with the sign inverted to make the comparison clear). When the factor $1/(1+2q^2)$ would be left out, the correspondence would be very bad indeed. Note that the factor $1 + 2q^2 \simeq 41$.

4. Conclusion

We compared the first results of turbulence measurements obtained with a new reciprocating Reynolds stress probe on TEXTOR to 2D-simulations of the Hasegawa–Wakatani model supplemented with curvature and neutral friction terms. The 2D model, without any temperature fluctuation, inevitably leads to underestimated values of the fluctuations and the transport of momentum. The cross correlation between density and potential being larger than in the real situation, we find a particle transport well in agreement with the experimental value. The influence of a realistic fraction of neutrals is marginal.

Our macroscopical model indicates that $m = 0$-background flows can indeed be driven by Reynolds stress, with a good agreement between theory and experiment only if the correct geometrical effects $(1 + 2q^2)$ are taken into account. Computing the poloidal acceleration from the experimentally measured Reynolds stress without this factor, one would overestimate its influence.

References

[1] P.H. Diamond et al., Phys. Fluids B 3 (7) (1991) 1626.
[2] S.-I. Itoh, Plasma Phys. Controll. Fusion 48 (2006) S1.
[3] Y.H. Xu et al., Phys. Rev. Lett. 84 (17) (2000) 3867.
[4] D. Biskamp et al., Phys. Rev. Lett. 74 (1995) 706.
[5] Y. Xu, J. Nucl. Mater., these Proceedings, doi:10.1016/j.jnucmat.2007.01.059.
[6] M. Vergote et al., Czech J. Phys. 55 (2005) 389.
[7] A. Hasegawa, M. Wakatani, Phys. Fluids 27 (1984) 611.
[8] B. Scott, Phys. Plasmas 12 (2005) 062314.
[9] M. Vergote et al., Plasma Phys. Controll. Fusion 48 (2006) S75.
[10] M. Harrison, Physics of Plasma–Wall Interactions in Controlled FusionNATO ASI of Series B, Vol. 131, Plenum Press, New York, 1986.
[11] D. Reiser, Phys. Plasmas 12 (2005) 122308.
[12] G.E. Karniadakis, J. Comput. Phys. 97 (1991) 414.
[13] Y. Xu et al., Phys. Rev. Lett. 97 (2006) 165003.
[14] Ch.P. Ritz et al., Rev. Sci. Instrum. 59 (8) (1988) 1739.
[15] S. Hirshman, Phys. Fluids 21 (1978) 224.
[16] J. Cornelis et al., Nucl. Fusion 34 (1994) 171.
[17] Ph. Mertens, J. Nucl. Mater. 241 (1997) 842.